CrossMark

Flame Heights and Heat Transfer in Façade System Ventilation Cavities

Karlis Livkiss* ⓘ, *Danish Institute of Fire and Security Technology, Jernholmen 12, 2650 Hvidovre, Denmark; Division of Fire Safety Engineering, Lund University, P.O. Box 118, 221 00 Lund, Sweden*

Stefan Svensson, Bjarne Husted and Patrick van Hees, Division of Fire Safety Engineering, Lund University, P.O. Box 118, 221 00 Lund, Sweden

Abstract. The design of buildings using multilayer constructions poses a challenge for fire safety and needs to be understood. Narrow air gaps and cavities are common in many constructions, e.g. ventilated façade systems. In these construction systems flames can enter the cavities and fire can spread on the interior surfaces of the cavities. An experimental program was performed to investigate the influence of the cavity width on the flame heights, the fire driven upward flow and the incident heat fluxes to the inner surfaces of the cavity. The experimental setup consisted of two parallel facing non-combustible plates (0.8×1.8 m) and a propane gas burner placed at one of the inner surfaces. The cavity width between the plates ranged from 0.02 m to 0.1 m and the burner heat release rate was varied from 16.5 kW to 40.4 kW per m of the burner length. At least three repeated tests were performed for each scenario. In addition, tests with a single plate were performed. The flame heights did not significantly change for $Q'/W < 300$ kW/m^2 (where Q' is the heat release rate per unit length of the burner and W is the cavity width). For higher Q'/W ratios flame extensions up to 2.2 times were observed. When the distance between the plates was reduced or the heat release rate was increased, the incident heat fluxes to the inner surface increased along the entire height of the test setup. The results can be used for analysing methodologies for predicting heat transfer and fire spread in narrow air cavities.

Keywords: Flame height, Heat flux, Flow velocity, Ventilated façade

1. Introduction

An air cavity between façade materials is in many cases a feature of modern building envelopes [1–4]. A ventilated building's external envelope typically consists of an exterior wall with mounted thermal insulation, a vapour barrier, an air cavity and an exterior cladding (e.g. rainscreen cladding). Such systems typically have a 0.02–0.06 m wide cavity for drainage and ventilation purposes. Mineral fibre and phenolic foams are commonly used as the insulation and high pressure laminates, metal sheets or ceramic tiles are used as the cladding material [2]. A

---

* Correspondence should be addressed to: Karlis Livkiss, E-mail: kal@dbi-net.dk

commonly considered 'worst case' building exterior fire spread scenario involves flames emerging from the windows of the room of fire origin after flashover. In façade fire scenarios, flames can interact with the outside cladding or may spread into the cavities between the façade material layers. The Knowsley Heights fire in 1991 is a noteworthy façade fire incident involving flame spread through the air cavity in rain screen cladding system [2].

In recent years, a number of research studies investigating the fire performance of ventilated façade systems had been done with full scale or reduced scale test rigs [1, 5–7]. It has been observed that the flames spreading up through an air cavity space of the building envelope can extend up to ten times higher compared to the flames outside the cavity [3] and that the presence of an air cavity contributes to increased burning rates of the cladding system [6].

From a fire safety perspective, it is important to both understand how the air cavity in these systems provides a pathway for the fire to spread up and, how it influences the ignition and the flame spread over combustible materials inside the cavity. To address the first of these points, the flame heights and the temperatures in different cavity arrangements should be investigated. For the latter point, the thermal exposure to the surfaces inside the cavity and oxygen availability should be investigated as important influential factors for the flame spread.

Research on fire scenarios inside narrow cavities is distinctly lacking. The purpose of this study is to provide additional data to the previously performed studies [8–11]. An experimental program was performed with an experimental setup, consisting of a propane line burner placed between two parallel facing walls. The visual flame heights, the flow velocities and the comparative incident heat fluxes to the cavity's inner surface were studied. In this study, the burner was located next to one of the walls to emulate a configuration where the flames are ejected next to or from the burning wall materials. The intention of this configuration was to provide data for analysing the heat transfer and the flame spread over the surface inside the cavity (e.g. over insulation materials or a vapour barrier). Up to six tests were performed for each experimental configuration to demonstrate the repeatability.

2. Background

Most of the research on fire plumes and flame spread in concealed spaces has been focused on rack storage arrangements. Karlsson et al. [8], Ingason [9], and Ingason and de Ris [10] performed experimental studies on two dimensional and three dimensional rack storage mock-ups. The main investigated parameters were the visual flame heights, the temperatures and the heat fluxes to the surfaces between the racks. The varied parameters in these studies were the burner heat release rate Q (usually presented per metre of burner length $Q' = Q/l$), the fuel type, and the distance between the storage racks. Inert materials were used to build the experimental setups. The geometrical parameter recognized to have the greatest influence was the distance between the rack 'columns', whereas the vertical distance between the levels of the racks arrays was shown to have little influ-

ence on the measured parameters [9]. In these studies Q was varied between approximately 18 kW to 147 kW and the horizontal separation distance between the racks was varied between 0.05 m and 0.15 m. Ingason developed a model for predicting the flame heights, the plume centre line temperatures, and the plume centre line velocities using a two dimensional approximation of the geometry [12]. Furthermore, Ingason performed free burning reduced scale (scale 1:3) and full scale tests with corrugated paper cardboard box arrays and measured the centre-line temperatures and gas velocities between the racks [13]. An investigation of heat fluxes to the surface in a two parallel plate configuration and in the middle of four modelled storage racks was done by de Ris and Orloff [14]. Several different fuels were used in these studies and it was shown that the heat flux from flames is sensitive to the flame sootiness.

Foley and Drysdale [11] measured heat fluxes to the inner surface between two parallel facing inert plates depending on the cavity width W (minimum 0.06 m), the burner location, the air flow conditions, and Q'. The study showed that the total heat flux to the surface increases as the cavity width is reduced. The study demonstrated the significance of the air flow conditions, which in this study were controlled by opening or closing the base of the test rig. The air availability had influence on the flame shape inside the gap. These tests were later used for model validation by Yan and Holmstedt [15]. Hu et al. [16] investigated flame heights between two parallel walls with cavity widths equal to and greater than 0.14 m, and different orientations of the line burner relative to the walls. Hu et al. found that in the investigated range the flame heights were not influenced by the cavity width when the long edge of the burner was perpendicular to the walls. In the cases where the burner long edge was parallel to the walls, the flame heights were found to increase when the cavity width was decreased.

In addition, a number of studies have been performed to investigate double skin façades exposed to flames emerging from a post-flashover compartment [17–20]. These studies demonstrated that the air cavity width plays a critical role determining the flame characteristics and the heat exposure to the surfaces inside the cavity.

In this study, an experimental program was performed to investigate the flame heights and the incident heat fluxes in cavities with W between 0.02 m and 0.1 m and Q' between 16.5 kW/m and 40.4 kW/m. The results were compared to the studies by Karlsson et al. [8] (W from 0.05 m to 0.2 m and Q' from 60 kW/m to 125 kW/m) and Ingason [9] (W from 0.05 m to 0.1 m and Q' from 32 kW/m to 74 kW/m).

3. Experimental

3.1. Experimental Setup

The experimental setup was comprised of two parallel facing non-combustible lightweight calcium silicate boards ($0.02 \times 0.8 \times 1.8$ m). The surfaces facing each other were lined with a 2 mm thick ceramic insulation layer. The ceramic insulation was used to increase the surface durability to fire impact, in order to allow more tests to be performed before changing the boards. No significant cracks or

smoke leakages through the boards occurred during the experimental work. A propane gas burner with an opening area of 8×391 mm, covered with a metallic mesh to uniformly distribute the gas flow, was placed in the middle of the cavity next to one of the calcium silicate boards. In this paper, the board with the burner next to it is referred to as the "near wall", whereas the other board is referred to as the "far wall". Additional tests were performed with the near wall alone and they're referred in this paper to as "one wall tests". The sides of the cavity were open, thus allowing air inflow. The experimental setup was designed in a way to contain the flames within the cavity between the walls. The main advantage of using a narrow burner was the possibility to use it for very narrow cavities. The experimental setup is shown in Fig. 1.

The experimental setup included the main elements of a construction system with an air cavity, however it did not include some important detailing of real life systems. In most cases real-life construction would be larger and it is likely that the air inflow along the sides would be restricted by physical obstructions. Similarly, if a rainscreen cladding system was considered, the cladding fixings would restrict the air flow also in the vertical direction. The setup in this study was chosen to investigate general flame behaviour and more applied research would require considerations of the construction detailing.

Three parameters were recorded during the test: the visual flame heights, the incident heat fluxes to the near wall surface and the flow velocity at the top of the experimental setup.

3.2. Flame Height Measurements

The visual flame heights L were measured from 30 photos taken with 1 s intervals during each test. The camera was placed on the side of the experimental setup with a view between the walls. A reference measurement photo with a levelling rod was taken each day prior to the experimental work to calibrate the camera position. The photos were taken starting at an arbitrarily chosen time of 130 s after the beginning of each test. The photos were taken late in the test (the duration of each test was 3 min), assuming that the flow had stabilized by that time. The reference photos were then visually compared to the photos from each test to determine the flame height. The average flame height from the 30 photos was calculated for each test, resulting in 30 s averaged measurements, and reported in this paper. Since the burner was relatively long, an assumption of the horizontal position of the flame tip was necessary. Based on the observations it was determined that the highest flame was in the middle of the burner. No distinction was possible between the flame heights across the length of the burner and different plume regions (i.e. persistent and intermittent regions) because of the narrow view angle inside the cavity.

The flame height in each photo was estimated with a precision of $\pm\, 0.05$ m. Additional measurement errors and uncertainties were present due to the sensitivity to the view angle of the camera, assumptions about the location of the flame tip along the burner length, and frequency of the flame oscillations relative to the camera shutter speed.
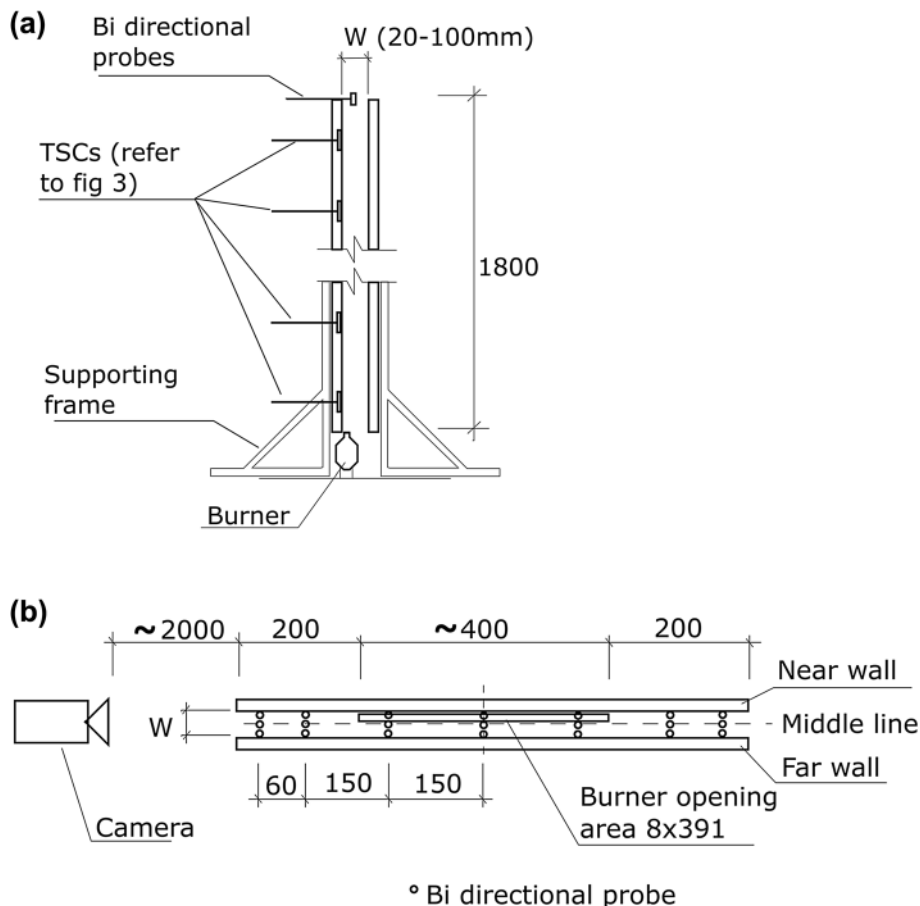
Figure 1. **Experimental setup (a) side view (b) top view. All dimensions given in mm.**

3.3. *Incident Heat Flux Measurements*

Custom-made thin skin calorimeters (TSCs) were designed and made to measure the incident heat fluxes to the near wall. The TSCs used in this study were similar to devices described by Häggkvist et al. [21], Hidalgo et al. [22], Tofilo et al. [23] and Wickström [24]. TSC is a robust and cost-effective device to assess the thermal impact to the surface. This device was chosen over the traditional heat flux gauges, because of its practicality.

TSCs were made of type K thermocouple wires soldered to a thin copper disc with a diameter of 40 mm and thickness of 0.2 mm. The back of the copper disc was insulated with rigid insulating fibre board (thickness 0.02 m) and flexible ceramic insulation (thickness 0.002 m). The TSCs were placed in circular holes drilled in the near wall and fixed with a 0.002 m thin sheet of plywood, stapled to the unexposed surface of the near wall. The TSC design is presented in Fig. 2.

In total, the near wall was instrumented with 45 TSCs as shown in Fig. 3. TSCs were placed in five columns with nine TSCs per column. The horizontal distance between TSC columns was 0.1 m and the vertical distance was 0.2 m. Due to the large amount of measurements, data only from nine TSCs located at the centre-line is presented in this paper. It was assumed that the incident heat flux distribution along the centreline was the least influenced by the incoming air from the sides and therefore was the most appropriate for drawing general conclusions.

The incident heat fluxes were back-calculated from the transient TSC temperature measurements. It was assumed that $\dot{q}''_{inc}$ was constant during each individual test. The calculations were done with the finite element program COMSOL Multiphysics®. Equation 1 was solved with the boundary conditions presented in Eqs. 2 and 3:
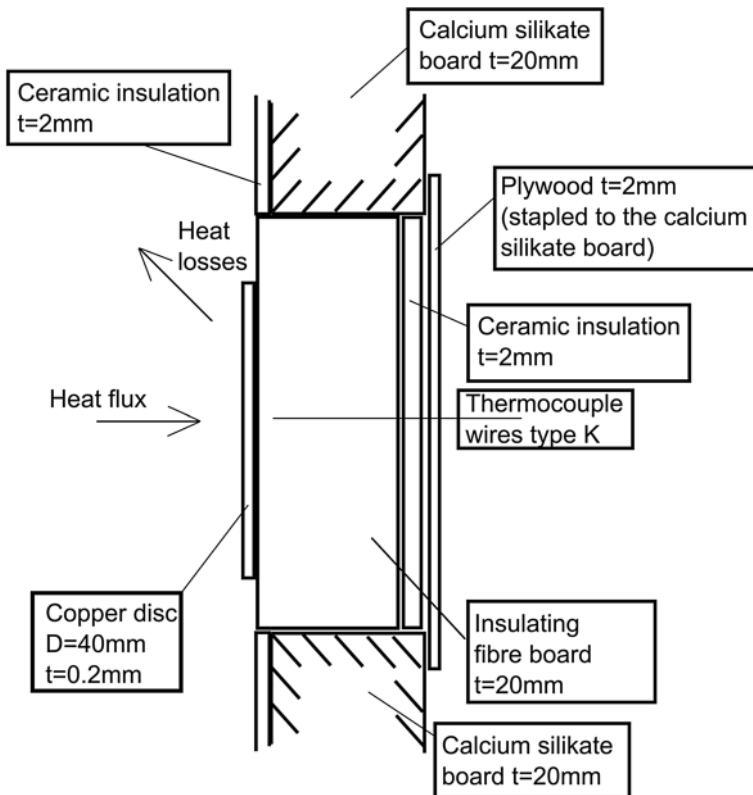

Figure 2.   Thin skin calorimeter TSC used in this study (t—thickness, D—diameter).
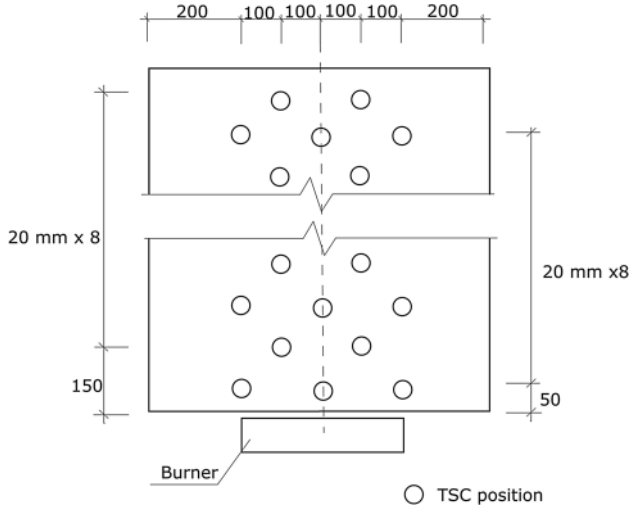
Figure 3. Locations of TSC on the near wall. All dimensions given in mm.

$$\rho c_p \frac{\partial T}{\partial t} = \frac{\partial}{\partial x}\left(k \frac{\partial T}{\partial x}\right) \qquad (1)$$

$$\dot{q}_h'' = \alpha \dot{q}_{inc}'' - \varepsilon \sigma T_s^4 \qquad (2)$$

$$\dot{q}_c'' = h(T_s - T_\infty) \qquad (3)$$

where ρ, c_p, k are the density (kg/m^3), the specific heat (J/(kg K)) and the thermal conductivity (W/(m K)) of each TSC material layer (copper, insulation and plywood), $\dot{q}_h''$ and $\dot{q}_c''$ are the net heat fluxes per unit area (W/m^2) at the exposed and unexposed boundary, ε is the emissivity (–), α is the absorptivity (–), h is the convective heat transfer coefficient (W/(m^2 K)), T_s is the surface temperature (K), T_∞ is the ambient temperature (= 293.15 K), $\dot{q}_{inc}''$ is the incident heat flux (sum of incoming radiation and convection) per unit area (W/m^2), σ is the Stefan–Boltzmann constant (= 5.67×10^{-8} W/(m^2 K^4)). The numerical model was run for incident heat fluxes from 1 kW/m^2 to 80 kW/m^2, with a step of 1 kW/m^2, resulting in 80 simulations. TSC response (the copper disc temperature) during 3 min of exposure was calculated. Three minutes was also the duration of each individual test in the parallel wall experimental program.

The temperature measurements taken during the experimental program were compared to the numerically predicted temperatures. The comparison was done by calculating the Euclidean relative distance (ERD) value [25–27]. ERD is the sum of differences between the model and the test results for each time step. The ERD calculation is given in Eq. 4:

$$\text{ERD} = \frac{\|\mathbf{T}_M - \mathbf{T}_E\|}{\|\mathbf{T}_M\|} = \frac{\sqrt{\sum_{i=1}^{n} \left(\mathbf{T}_{M,i} - \mathbf{T}_{E,i}\right)^2}}{\sqrt{\sum_{i=1}^{n} \left(\mathbf{T}_{M,i}\right)^2}} \tag{4}$$

where the subscripts M and E refer to the model and the test values respectively. A lower ERD value indicates that the modelled TSC response to the incident heat flux is closer to the TSC measurements in the parallel wall experiments.

This methodology required that the thermal properties of the TSC materials were well known. To validate the TSC material properties, the numerical heat conduction model (solving Eq. 1) was first compared with temperature measurements in the cone calorimeter apparatus [28] using horizontal orientation specimens with irradiances of 60, 50, 40, 30, 20, 10, 5, 2 and 1 kW/m^2. The cone calorimeter was calibrated with a Schmidt–Boelter gauge each time the irradiance was changed. A combined radiation and convection boundary condition was applied on the exposed surface (Eq. 5) and an insulated boundary condition on the unexposed side (Eq. 6):

$$\dot{q}_h'' = \alpha \dot{q}_r'' - \varepsilon \sigma T_s^4 + h(T_\infty - T_s) \tag{5}$$

$$\dot{q}_c'' = 0 \tag{6}$$

where $\dot{q}_r''$ is the irradiance from the cone heater (W/m^2).

In validation tests the copper discs were covered with a layer of black paint before each test, and in modelling $\alpha = \varepsilon = 1$ was assumed. The black paint was used to correct the measurements for the soot that was observed to accumulate on the copper discs during the parallel wall tests. The convective heat transfer coefficients used in the validation study were taken from the SFPE handbook [29], and linearly extrapolated for irradiances below 20 kW/m^2. The modelling results gave good match with the cone calorimeter test results as shown in Fig. 4. The TSC material properties used in this study are presented in Table 1.

An implicit assumption in this methodology was that the calculated $\dot{q}_{inc}''$ (the sum of incoming radiation and convective heat flux) in parallel wall experiments was constant throughout the whole duration of each test. The convective heat transfer coefficient at the unexposed surface of the TSC, i.e. the back of the plywood, was assumed to be 5 W/(m^2 K). The temperature rise on the unexposed surface exposed to 80 kW/m^2 for 3 min was only 4 K), therefore the radiation losses on the unexposed surface were ignored. The copper disc emissivity was assumed to be constant $\varepsilon = 1$ (Kirchhoff's law for grey surfaces applies). This assumption was made because it was observed that soot quickly accumulated on the copper disc during the tests. The thermal properties and the thickness of the soot layer were however disregarded in the analysis. It was also assumed that all materials were in a perfect thermal contact and the analysis was limited to one dimensional heat transfer. This simplified method for calculating $\dot{q}_{inc}''$ was chosen to systematically analyse the extensive amount of experimental data. Because of
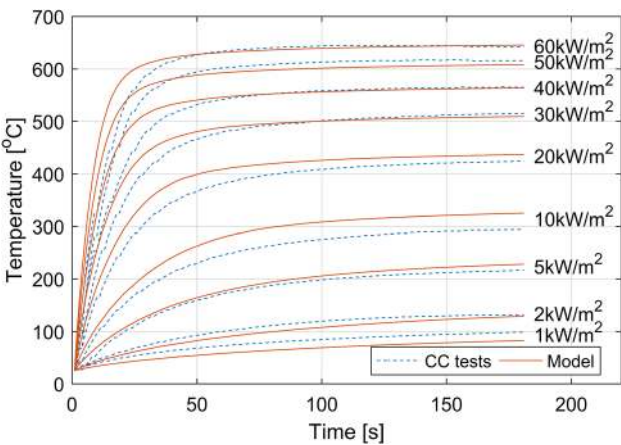
Figure 4. TSC exposed surface temperature in calibration tests with cone calorimeter and model predictions.

Table 1
TSC Material Properties

Material	Thermal conductivity, k (W/(m K))	Specific heat, c_p (J/(kg K))	Density, ρ (kg/m^3)	Surface emissivity, ε and absorptivity, α (–)	Thickness, L (m)
Copper	400	$0.1035T + 354.94$	8667	1	2×10^{-4}
Insulation	0.05	1074	270	Not used	2×10^{-2}
Plywood	0.12	1215	545	Not used	2×10^{-3}

the assumptions, $\dot{q}''_{inc}$ should be used for relative comparison between the experimental cases rather than "real" values.

The main sources of the measurement errors and uncertainties as reported by equipment providers are the thermocouple deviation (max $-$ 0.5°C in range 0–400°C), uncertainty of the thermocouple temperature readings (the highest absolute value of $\pm$ 0.3% and $\pm$ 1 K) and the accuracy range of the data acquisition system (1°C between $-$ 100°C and 600°C). The uncertainties in the $\dot{q}''_{inc}$ calculation results due to these measurement uncertainties and errors are discussed in Sect. 4.2. Other sources of the uncertainty are associated with the calibration tests, including the radiative heat flux from the cone calorimeter, assumptions about convective heat transfer, and TSC material properties.

3.4. Outflow Velocity Measurements

Vertical outflow velocities were measured at the top of the experimental setup with bi-directional probes with diameter of 0.016 m [30]. These measurements were done for another ongoing study focusing on validation of Computational

Fluid Dynamics CFD model for this test condition and are of secondary importance for this paper.

The vertical flow velocity measurements were performed for the experimental series I, II and III with $W = 0.04$ m, for the experimental series II with $W = 0.02$ m and for the experimental series IV with $W = 0.1$ m. Only four bi-directional probes were available for this study and, thus, to cover the entire outflow area, repeated tests were performed for the same W and Q' with the probes in various locations. Using this approach, measurements at 21 locations (see Fig. 1b) were taken during six repeated tests. An exception to this was the velocity measurements for the tests with $W = 0.02$ m, in which, due to the narrow cavity, measurements only along the middle line of the cavity were done.

The flow velocities were calculated with Eq. 7:

$$v = \frac{\sqrt{\frac{2\Delta P}{\rho_g}}}{C} \tag{7}$$

where ΔP is the pressure difference (Pa) measured with the bi-directional probes, C is the Re number dependent probe response coefficient (–) [30], ρ_g is the gas density (kg/m^3) calculated with the ideal gas law, and v is the velocity (m/s).

The accuracy of the C calculated as a function of Re number is reported to be approximately 5% and the inclination angle of the bi-directional probe up to 50° will create a difference of the mean velocity measurement of up to $\pm$ 10% [30]. Additional uncertainties may be created by the transient heating of the walls [31]. Bi-directional probes in this experimental setup were used in spaces comparable to the probe diameter (probes with d = 0.0016 m were used in the 0.02 m cavity). Errors in measurements may therefore also be due to the velocity flow profiles in the cavity and the influence of the boundary layer. Computational fluid dynamics programs (e.g. Fire Dynamics Simulator) could be used to estimate the errors created by the flow profile gradient.

3.5. Description of the Experimental Program

The experimental program consisted of four experimental series (experimental series I–IV), with a different propane gas mass flow, resulting in a different heat release rate HRR. The mass flow was changed before each experimental series and maintained for the duration of the experimental series without modification. In total, 77 individual tests were performed during the experimental program. Each individual test was 3 min long. The full experimental program is summarized in Table 2.

Minor changes of the HRR during the same experimental series were observed. To quantify these inconsistencies the HRR was monitored during the individual tests. The heat release rate was calculated as the average value during time for 10 l propane (in the experimental series I) or 20 l propane (in the experimental series II, III and IV) to be consumed. The propane mass flow to the burner was monitored with a diaphragm gas flow meter from Elster Handel GmbH Mainz and the gas pressure was monitored with a liquid column monometer type pres-

Table 2
Overview of the Experimental Program

Experimental series (ES)	Average Q' (kW/m)	Cavity width, W (m)	Number of individual tests		
			Flame heights	$\dot{q}''_{inc}$	Outflow velocity measurements (different scenarios)
I	16.5	0.1, 0.06, 0.05, 0.04, 0.03, 0.02, one wall	19	22	1 (W = 0.04 m)
II	24.8	0.1, 0.06, 0.05, 0.04, 0.03, 0.02, one wall	23	23	2 (W = 0.04 m and 0.02 m)
III	32.3	0.1, 0.06, 0.05, 0.04, 0.03, one wall	16	19	1 (W = 0.04 m)
IV	40.4	0.1, 0.06, 0.05, 0.04, one wall	12	13	1 (W = 0.04 m)
		Total	70	77	5

Table 3
Q' Distribution During the Experimental Series I and Series III

Experimental series (ES)	Min Q' (kW/m)	Mean Q' (kW/m)	Max Q' (kW/m)	Max variation compared to the mean (%)	Standard deviation (kW/m)	Based on (number of individual tests)
I	15.6	16.5	18.2	10	0.6	21
III	31.8	32.3	32.8	2	0.3	19

sure meter. The burner HRR was calculated from the propane mass flow and corrected for the propane gas pressure and temperature. The propane heat of combustion was assumed to be 46.45 kJ/g. The heat release rate was monitored for all the individual tests during the experimental series I and III. The variations in the HRR are presented in Table 3.

The main measurement errors and uncertainties in the HRR measurements were due to the gas flow meter and the pressure meter readings. The main contribution to the gas flow meter uncertainty was the measurement deviation (maximum 2%) and the visual measurement uncertainty (estimated maximum 1% based on one measurement step). The main contribution to the errors and uncertainties from the pressure meter was the visual measurement uncertainty (estimated maximum 4% based on one measurement step). The total HRR uncertainty was calculated to be 3%. The maximum differences in the measured Q' between the repeated tests was 10%, as shown in Table 3, and because it was higher than the estimated measurement uncertainty, it was suggested that the uncertainty of the propane gas flow from the source was relatively high.

4. Results

4.1. *Flame Heights*

The experimental setup allowed containing the entire flame between the walls—no flames were emerging outside along the sides or above the walls. With cavity widths of 0.04 m and greater and low Q' the flames did not fill the entire cavity width. In these tests, turbulent eddies in the flame structure were visually observed. As the cavity width was reduced the plume flow appeared to be more vertically oriented and the flames filled the entire cavity width. The transition to the mode where the flames filled the entire cavity width was observed to occur at the cavity width of 0.03 m in the experimental series I, II and III and at 0.04 m in the experimental series IV. The visual observations clearly indicated that the flame heights increased with reduced W. An example of the flame structure is presented in Fig. 5.

The results of average visual flame height measurements are presented in Figs. 6 and 7, where the average data of the repeated individual tests are presented together with the measurement errors and uncertainties. The errors and uncertainties are based on 10% uncertainty for Q' (see Table 3) and flame height measurement uncertainty of 0.05 m. The format of Figs. 6 and 7 is based on work by Karlsson et al. [8] and Ingason [9]. The experimental setup in the previous studies had different ranges of cavity width and Q' as described in Sect. 2. In previous studies the burner was located in the middle of both walls and had horizontal air inlet flues at multiple heights of the setup. The purpose of presenting the results from this study in a similar way is to provide an easy comparison between the studies.

The data in Fig. 6 is presented together with results from the study by Karlsson et al. [8]. Karlsson et al. studied the flames between the storage racks. In addition to the horizontal separation between the obstructions, Karlsson et al. also used vertical separations between the 'boxes'. A linear relation of the flame height to the $Q'^{2/3}$ had been previously suggested by Hasemi et al. [32] for burners with
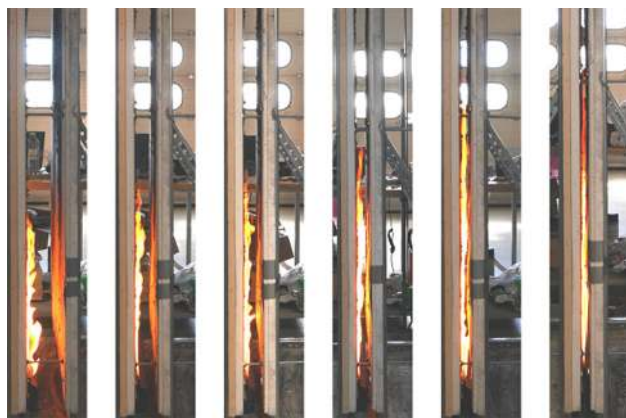

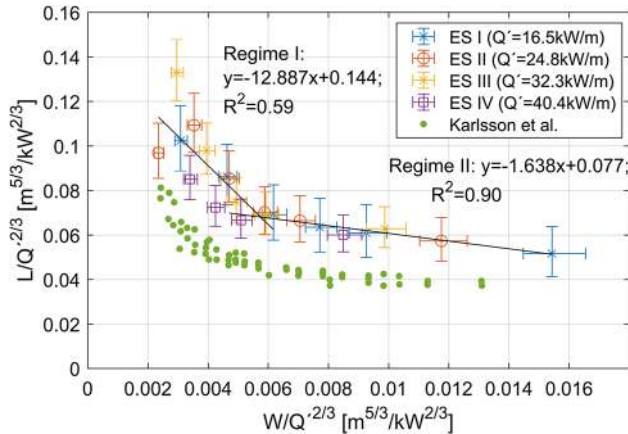**Figure 5. Photos of the experimental series II. From left hand side W = 10, 6, 5, 4, 3 and 2.**

Figure 6. **Average flame heights in this study and Karlsson et al. [8], and linear correlations. Error bars show measurement uncertainties.**
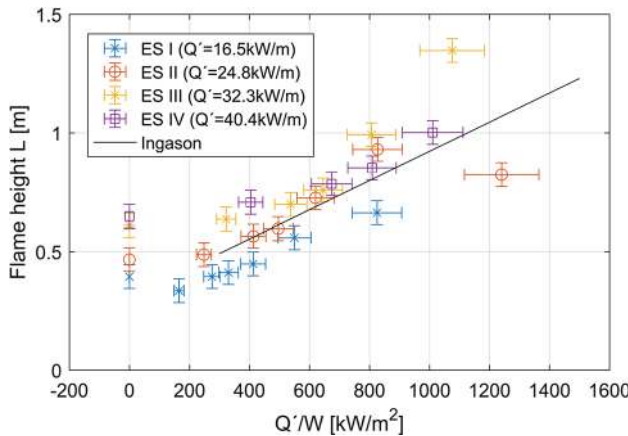

Figure 7. **Average flame height data compared with linear correlation given by Ingason L = 0.307 + 6.15E − 4(Q'/W) [9]. Error bars show measurement uncertainty.**

large aspect ratios and this relationship was also used by Karlsson et al. This study showed approximately 50% higher flames compared to Karlsson et al. and one of the possible explanations is the effect of the burner location. In the study by Karlsson et al. the burner was located on the middle line of the cavity and the air inflow was provided from both longitudinal sides of the burner. In this study, the burner was located next to one of the walls and the air entrainment was possible from only one longitudinal side. Despite the differences in the experimental setups and the absolute values of the results, both studies showed very similar patterns when $W/Q'^{2/3}$ was plotted versus $L/Q'^{2/3}$. For values of $W/Q'^{2/3} < 6 \times 10^{-3}$ $m^{5/3}/kW^{2/3}$ more scatter in the results was observed, suggesting different regimes

and dependency between the parameters than in tests with a higher $W/Q'^{2/3}$ ratio. Linear correlations were proposed and given in Fig. 6 for regime I ($W/Q'^{2/3} < 6 \times 10^{-3}$ m$^{5/3}$/kW$^{2/3}$) and regime II ($W/Q'^{2/3} > 6 \times 10^{-3}$ m$^{5/3}$/kW$^{2/3}$).

In Fig. 7, the visual flame heights from this study are compared with the previous study by Ingason [9]. Ingason used a similar storage rack setup as Karlsson et al.; however, Ingason also closed the sides of the experimental setup to restrict the incoming air inflow. Comparison of the average flame heights in this study with Ingason's proposed linear correlation resulted in a maximum error of 39%. As shown in Fig. 7, the tests with lower Q' resulted in lower flame heights compared to the tests with higher Q' (e.g. the experimental series I gave, in general, lower flames than the experimental series II, III and IV). When presented in this form, the results were scattered, indicating that the Q'/W ratio is not a sufficient parameter to correlate the flame heights with. The flame height did not significantly change below $Q'/W < 300$ kW/m^2. The maximum observed flame extension was 2.2 times in ES III.

The repeatability of the flame height measurements are presented in Fig. 8. The difference between the individual test measurements and the average value for repeated tests was less than 10%.

4.2. Incident Heat Flux at the Centreline to the Near Wall

Incident heat fluxes $\dot{q}''_{inc}$ to the near wall were calculated as described in Sect. 2 and the results are presented in Figs. 9, 10, 11, 12, 13, 14, 15 and 16.

Minor asymmetry of $\dot{q}''_{inc}$ was observed as presented with an example in Fig. 9. Asymmetrical flame could be created by the air drafts from the sides of the experimental setup or by the burner design. The propane gas was fed into the burner from one side only, and it could cause a non-uniform pressure distribution inside the burner and therefore the propane gas release would not be uniform over the
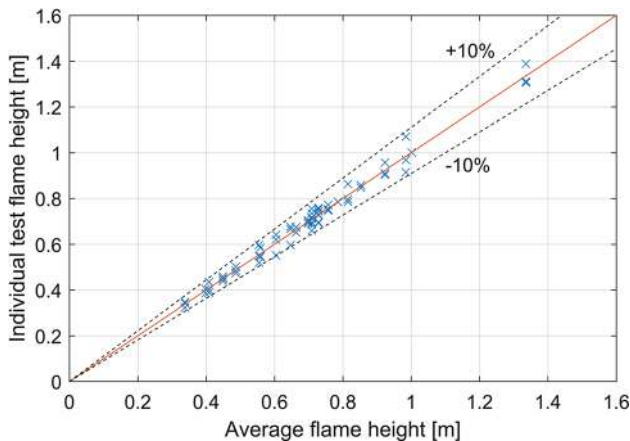

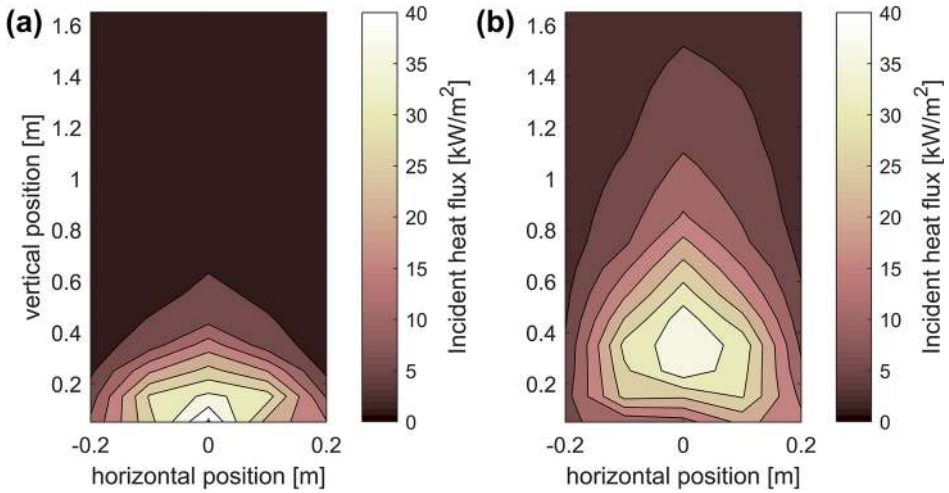**Figure 8.   Repeatability of flame height measurements.**

Figure 9.   Incident heat flux distribution examples. Values between the TSC device locations were linearly interpolated. (a) ES I $W = 0.05$ m, (b) ES IV $W = 0.05$ m.

length of the burner. To further improve the experimental setup a burner with multiple, symmetrically located, gas inflow tubes should be used.

The centreline $\dot{q}''_{inc}$ measurements showed that reducing the cavity width resulted in higher incident heat fluxes along the entire height of the near wall. An increase of $\dot{q}''_{inc}$ to the inner cavity surface with a reduction of the cavity width was also reported by Foley and Drysdale [11].

In addition to the flame radiation, $\dot{q}''_{inc}$ could be also affected by the radiation heat feedback from the far wall. Even though the test duration was only 3 min, the far wall would have an influence on the heat balance of the TSCs. Furthermore, more enclosed space may create more sooty flames due to the limited availability of oxygen and thus increased radiation from the flames.

Figure 10 shows that $\dot{q}''_{inc}$ was lower at 0.05 m above the burner, compared to the location 0.25 m above the burner during the experimental series II, III and IV. This observation may be explained by a possible flame lift off from the burner, a small air gap between the burner and the near wall, or a measurement error.

As shown in Figs. 11 and 12, in general, higher Q' resulted in higher $\dot{q}''_{inc}$ values. However, in some cases, the experimental series II to IV gave comparable results and, in some cases, the $\dot{q}''_{inc}$ was lower for experimental series IV than other experimental series.

Figure 13 shows an increase in $\dot{q}''_{inc}$ in parallel wall tests, relative to the one wall test. Measurements below and above the one wall test flame height are presented separately. The former shows an increase of $\dot{q}''_{inc}$ related to the flame properties (e.g. sootiness), whereas the latter is related to the flame height increase. In all cases, an additional contribution to the $\dot{q}''_{inc}$ is due to the heat feedback from the
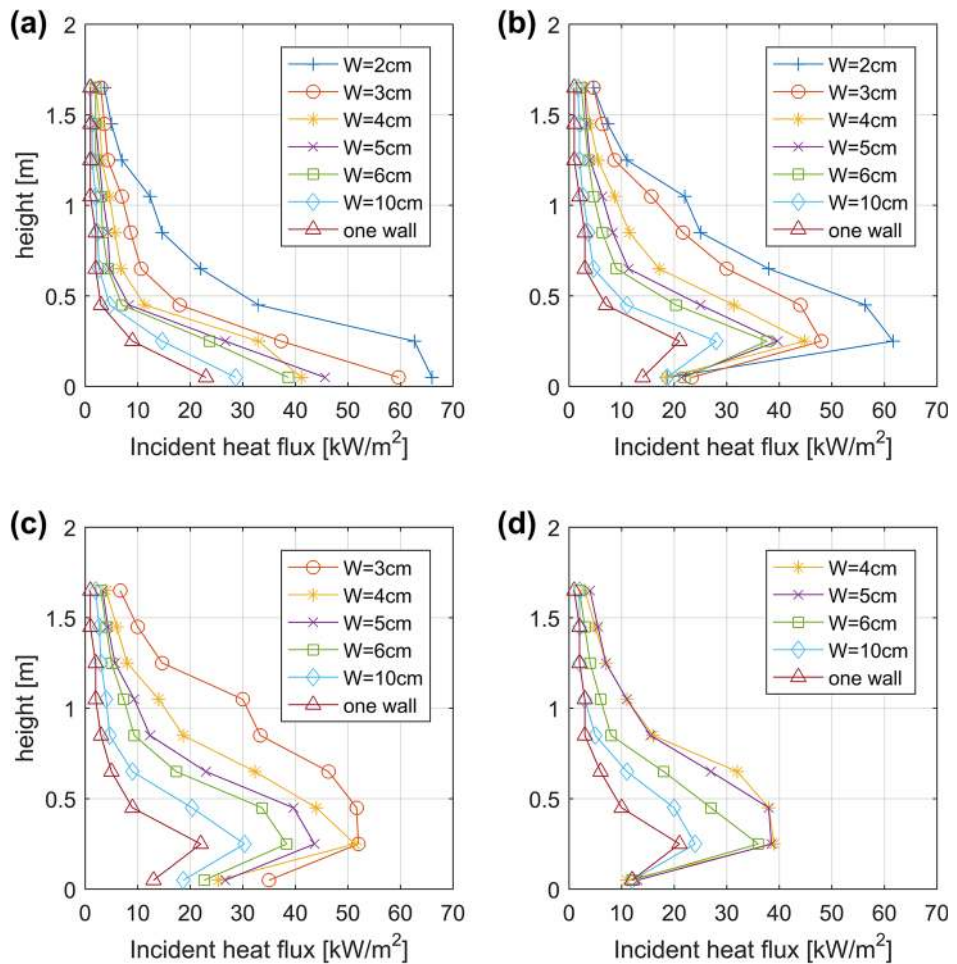
Figure 10. **Incident heat fluxes at the centreline of the near wall**
(a) ES I ($Q' = 16.5$ kW/m), (b) ES II ($Q' = 24.8$ kW/m), (c) ES III
($Q' = 32.3$ kW/m), (d) ES IV ($Q' = 40.4$ kW/m).

far wall. The incident heat flux increased on average 4.4 and 8.6 times for measurements below and above the flame height in the one wall test. The maximum observed $\dot{q}''_{inc}$ increase was 15 times.

The repeatability of the incident heat flux measurements is presented in Fig. 14, where the average measurement values from the repeated tests are compared to the individual test measurements. With an exception of one outlier, the largest difference between the individual test measurements and the average values for the repeated tests was less than 25%.

The calculations of $\dot{q}''_{inc}$ were based on comparison of the TSCs' temperatures in parallel wall tests and FEM model under constant incident heat flux. The compar-
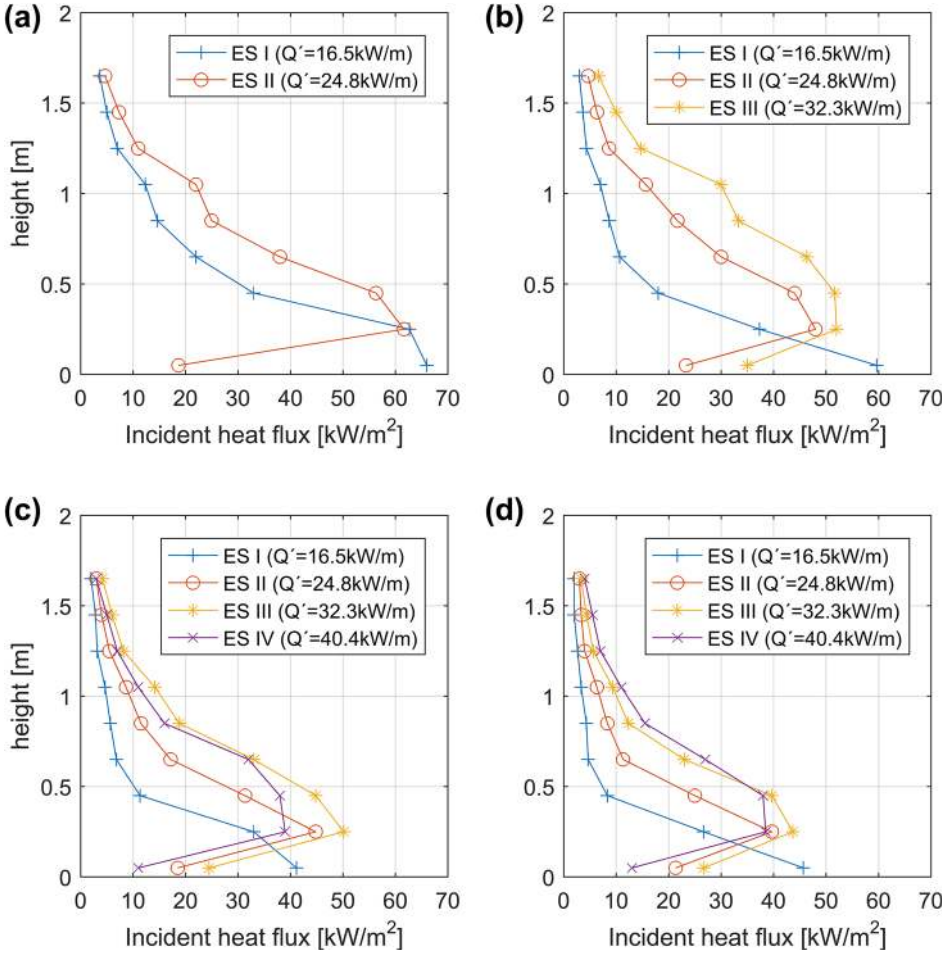
Figure 11. Incident heat fluxes (a) W = 0.02 m, (b) W = 0.03 m, (c) W = 0.04 m, (d) W = 0.05 m.

ison was done by calculating ERD value (Eq. 6), where low ERD values indicate a good match. ERD values are presented in Fig. 15. Most of the ERD values are below 0.1 (less than 10% temperature difference between the model and test).

The uncertainty of calculated $\dot{q}''_{inc}$ were investigated based on the measurement errors and uncertainties presented in Sect. 3.3. The uncertainties are presented in Fig. 16. In most cases the temperature measurement errors did not significantly influence the resulting $\dot{q}''_{inc}$, and the maximum calculated deviation was 3 kW/m². Since the measurement uncertainty was low compared to the variation in the repeated tests, it was concluded that the experimental results were more influenced by factors, such as repeatability of the burner HRR and laboratory conditions.
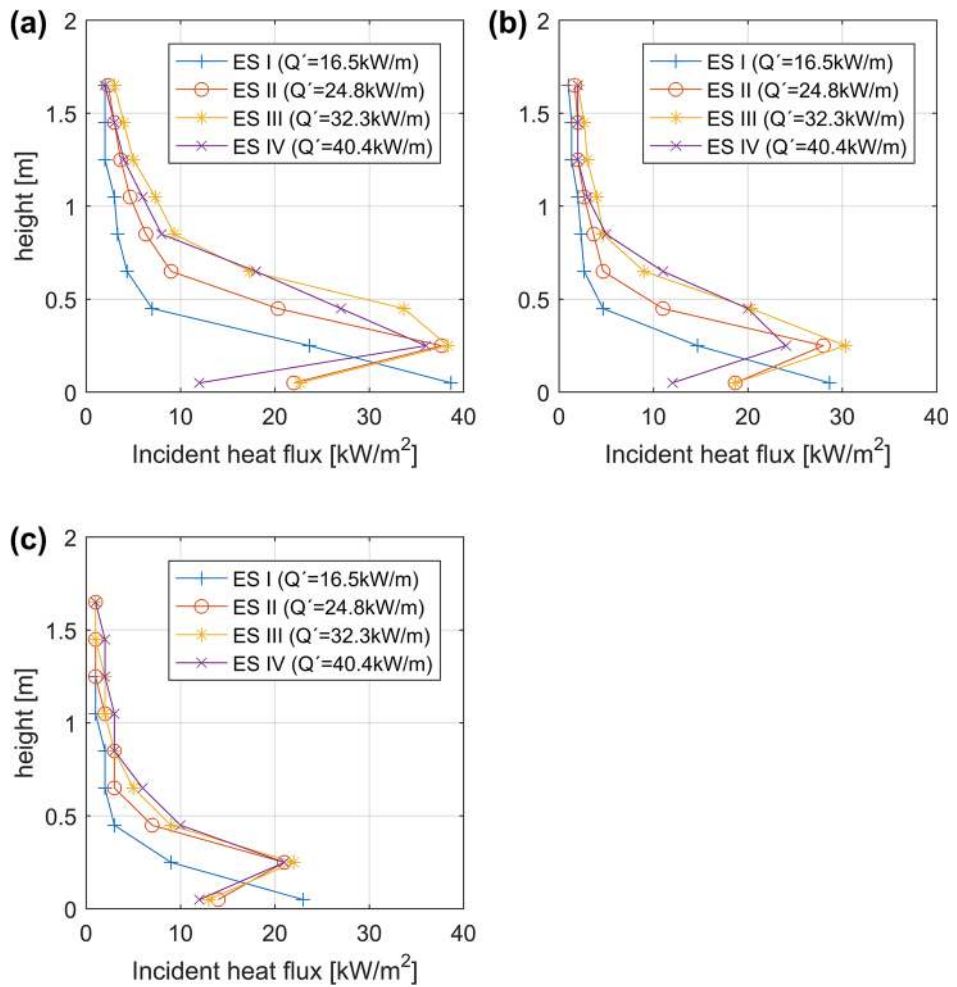
Figure 12. **Incident heat fluxes (a) W = 0.06 m, (b) W = 0.1 m, (c) one wall.**

4.3. Outflow Velocity

The vertical outflow velocity was measured in various locations above the cavity. From the measurements, it was concluded that the gas flow velocity became relatively steady a few seconds after the beginning of each test. The average outflow velocities were calculated from the final minute of each test and are presented in Figs. 17 and 18.

Figure 17 shows the outflow velocities in the experimental series I, II, and III with $W = 0.04$ m at the top of the cavity in three positions: at the near wall, middle line, and far wall. As presented in Fig. 17 the outflow velocity at the top of the experimental setup was close to uniform over the cavity width. However, the
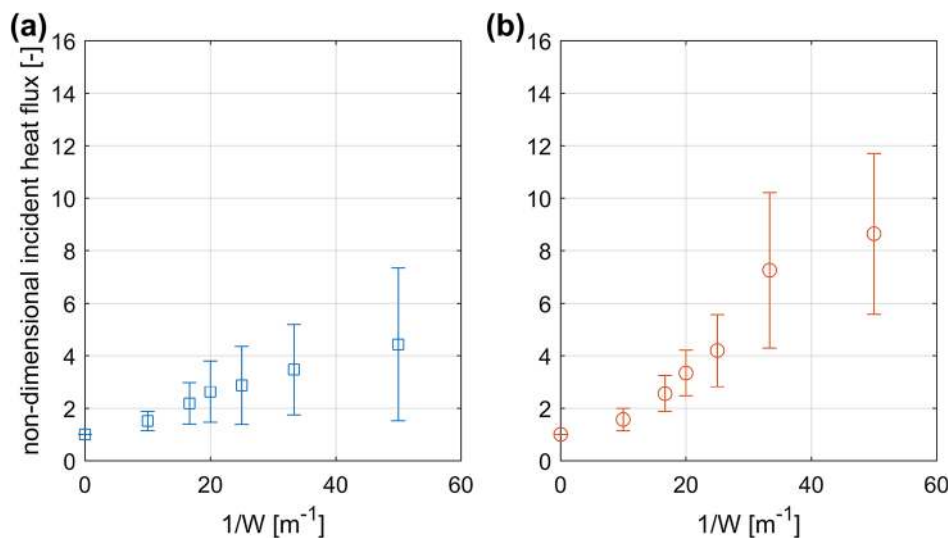
Figure 13. **Relative incident heat flux increase as a function of cavity width (a) below the one wall flame height, (b) above the one wall flame height. Error bars show two standard deviations around the mean value.**
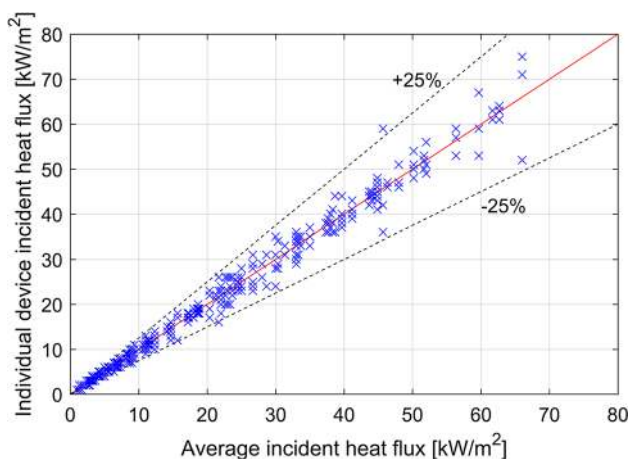
Figure 14. **Repeatability of the individual incident heat flux measurements.**

outflow velocity significantly changed over the length of the cavity. Up to 40% difference was observed between the experimental series I and III.

Figure 18 shows the outflow velocity in the centre of the cavity as a function of Q'/W. The outflow velocity increased linearly for the same W when the burner HRR was increased. The results showed that for the experimental series II reduc-
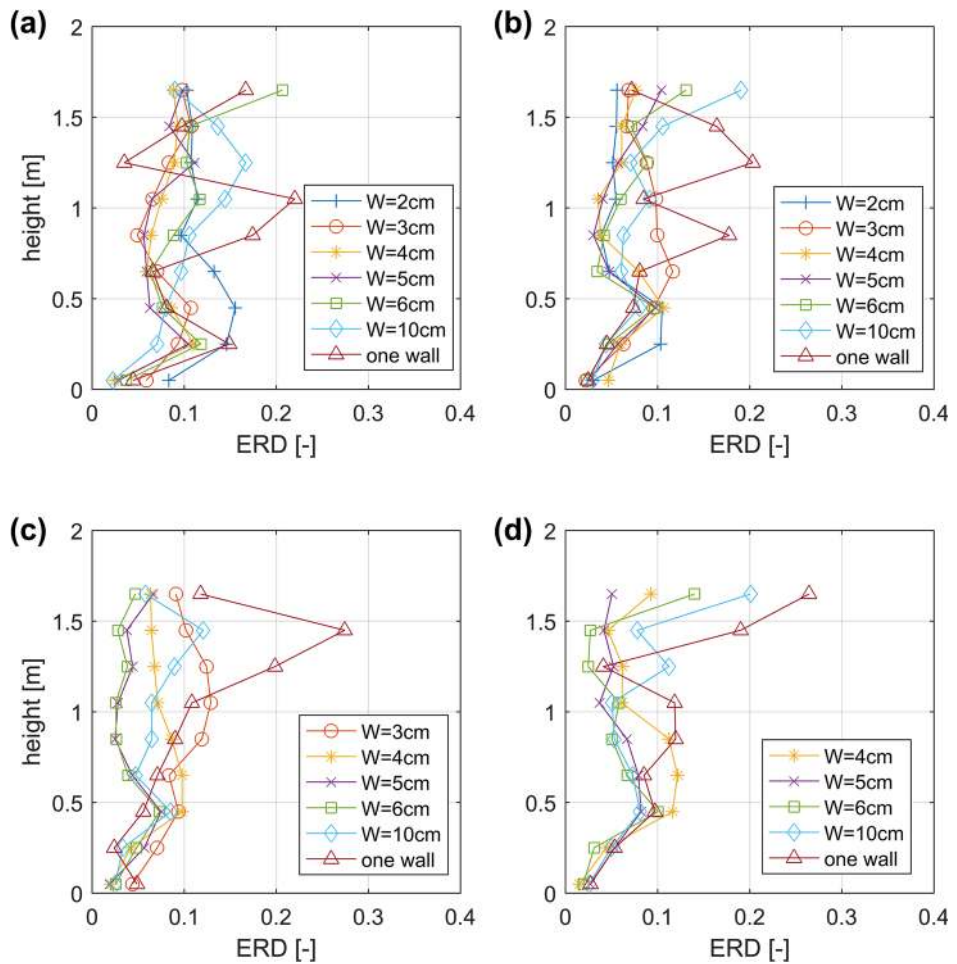
Figure 15.   Average ERD values from repeated tests.

ing cavity width from 0.04 m to 0.02 m did not significantly influence the outflow velocity for the same burner output.

Repeated outflow velocity measurements were done only for the centreline positions. In the experimental series IV $W = 0.1$ m the repeatability of these measurements was 21%, whereas in all the other tests the difference between the two measurements was less than 9%.

5. Conclusions

The influence of the air cavity width between two inert parallel facing plates on the diffusion flame heights and incident heat fluxes to the inner surface was stud-
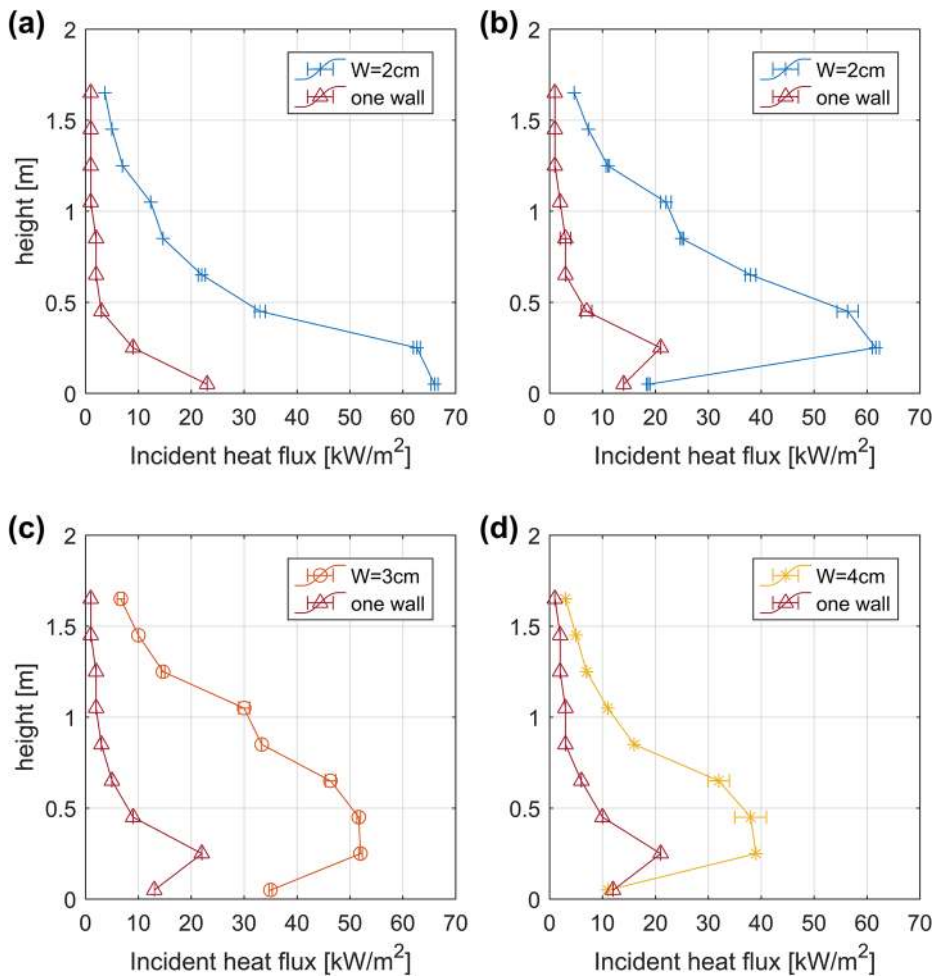
Figure 16. **Incident heat flux measurement uncertainties.**

ied. The results showed that the flame height was relatively constant for $Q'/W < 300$ kW/m^2. For higher Q'/W ratios, the flame extension was observed to be up to 2.2 times, when compared to the one wall test. The results showed up to 50% higher flames than those reported in previous research by Karlsson et al. [8]. This inconsistency could be explained by the fact that Karlsson et al. used a burner in the middle of the cavity, while in this study, it was placed next to the near wall. Furthermore, different burner widths could also create inconsistent results between both studies. A wider burner would result in a larger gas outlet area, therefore lower gas outflow velocity and lower flame heights. However, the burner width used in the study by Karlsson et al. [8] was not reported. Nevertheless, the flame height as a function of the cavity width followed a very similar pattern in
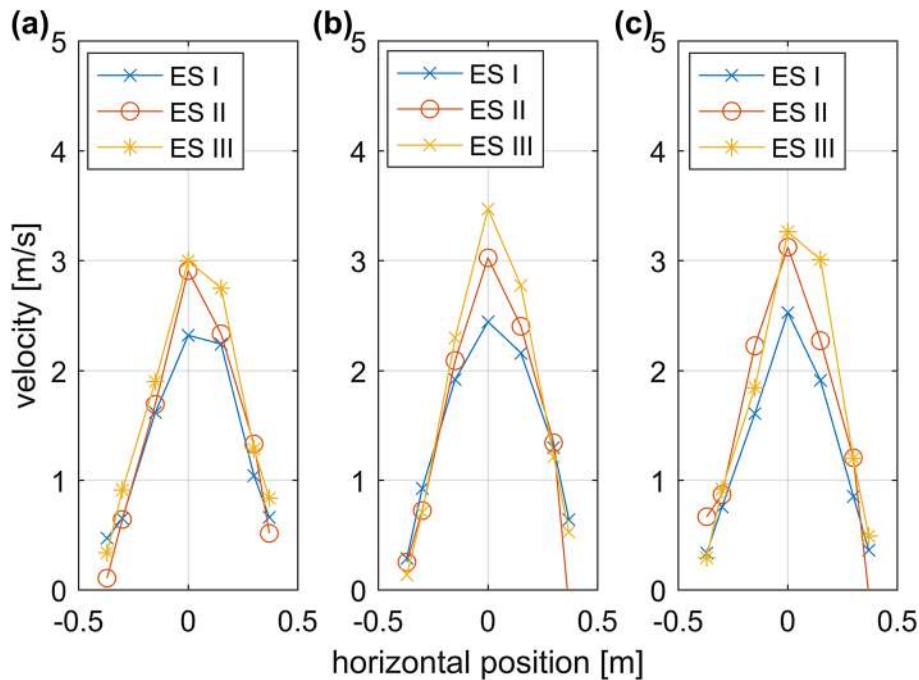
Figure 17. Outflow velocity measurements for W = 4 cm (a) near wall, (b) middle line, (c) far wall.
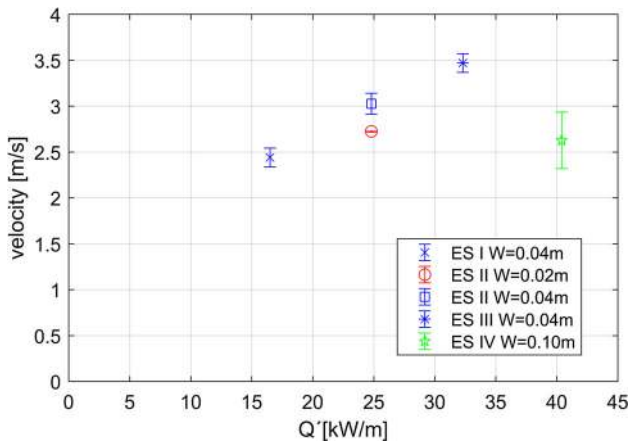

Figure 18. Outflow velocity at the centre of the cavity. Error bars show range of measurements in repeated tests.

both studies, indicating that the same underlaying mechanisms applies in both cases.

The incident heat fluxes were shown to increase over the entire height of the experimental setup, when the cavity width was decreased. A more severe heat exposure to the surface is therefore expected in the case of a cavity fire when, compared to a fire next to one wall.

The performed study provide data for investigating fire induced flows, heat transfer and flame spread modelling in vertically oriented air cavities. One of the fields of application is ventilated façade systems, for which numerical simulations and scale modelling should be investigated as a cost-effective screening method of façade performance before doing large scale physical testing. The results of this study provide data for the model validation and highlight the importance of the cavity width as an important parameter to be included in scale testing.

More investigations for application to ventilated façade systems should be undertaken to understand the mechanisms of flames entering the cavity and ways to prevent it. In future studies, construction details (e.g. cladding fixings), which may affect the flame spread within the ventilation cavity, should be included in small scale test design.

Acknowledgements

Open Access

References

1. Weghorst R, Hauzé B, Guillaume E (2016) Determination of fire performance of ventilated façade systems on combustible insulation using LEPIR2. Extended applications approach based on multiscale tests. In: Proceedings of 14th international fire and engineering conference Interflam, vol 2, pp 1139–1149
2. White N, Delichatsios M (2014) Fire hazards of exterior wall assemblies containing combustible components. The Fire Protection Research Foundation, Quincy
3. Colwell S, Baker T (2013) Fire Performance of external thermal insulation for walls of multistorey buildings, 3rd edn. IHS BRE Press, Garston
4. Strøm RA (2016) Recent progress on test evidence, standardization and design of protection for exterior openings. In: Proceedings of 2nd international seminar for fire

safety of facades, MATEC Web of Conferences. https://doi.org/10.1051/matecconf/20164601004

5. Kolaitis DI, Asimakopoulou EK, Founti MA (2016) A full-scale fire test to investigate the fire behaviour of the ventilated facade system. In: Proceedings of 14th international fire and engineering conference Interflam, vol 2, pp 1127–1138

6. Boström L, Skarin C, Duny M, McNamee R (2016) Fire test of ventilated and unventilated wooden façades, SP Report 2016:16. Borås

7. Jamison KLT, Boardman DA (2016) A new fire performance test for cavity wall insulation. In: Proceedings of 2nd international seminar for fire safety of facades, MATEC Web of conferences. https://doi.org/10.1051/matecconf/20164602004

8. Karlsson B, Thomas PH, Holmstedt G (1995) Flame sizes in a small scale stack: pilot experiments. Department of Fire Safety Engineering, Lund University, Lund

9. Ingason H (1994) Two dimensional rack storage fires. In: 4th international symposium of fire safety science, pp 1209–1220

10. Ingason H, de Ris JL (1998) Flame heat transfer in storage geometries. Fire Saf J 31:39–60. https://doi.org/10.1016/S0379-7112(97)00062-3

11. Foley M, Drysdale DD (1995) Heat transfer from flames between vertical parallel walls. Fire Saf J 24:53–73. https://doi.org/10.1016/0379-7112(94)00033-C

12. Ingason H (1998) Modelling of a two-dimensional rack storage fire. Fire Saf J 30:47–69. https://doi.org/10.1016/S0379-7112(97)00024-6

13. Ingason H (2001) Plume flow in high rack storages. Fire Saf J 36:437–457. https://doi.org/10.1016/S0379-7112(01)00007-8

14. de Ris JL, Orloff L (2005) Flame heat transfer between parallel panels. In: Proceedings of 8th international symposium of fire safety science, pp 999–1010

15. Yan Z, Holmstedt G (1999) Three-dimensional computation of heat transfer from flames between vertical parallel walls. Combust Flame 588:574–588. https://doi.org/10.1016/S0010-2180(98)00092-3

16. Hu L, Liu S, Zhang X (2017) Flame heights of line-source buoyant turbulent non-premixed jets with air entrainment constraint by two parallel side walls. Fuel 200:583–589. https://doi.org/10.1016/j.fuel.2017.03.082

17. Chow NCL, Han SS (2015) A study on building-integrated photovoltaic system fire with double-skin façade by scale modeling experiment. In: 2nd European symposium of fire safety science

18. Chow WK, Hung WY (2006) Effect of cavity depth on smoke spreading of double-skin facade. Build Environ 41:970–979. https://doi.org/10.1016/j.buildenv.2005.04.009

19. Chow CL (2011) Numerical studies on smoke spread in the cavity of a double-skin facade. J Civ Eng Manag 17:371–392. https://doi.org/10.3846/13923730.2011.595075

20. Li J, Xing X, Hu C et al (2012) Numerical studies on effects of cavity width on smoke spread in double-skin facade. Proc Eng 45:695–699. https://doi.org/10.1016/j.proeng.2012.08.225

21. Häggkvist A, Sjöström J, Wickström U (2012) Using plate thermometer measurements to calculate incident heat radiation. J Fire Sci 31:166–177. https://doi.org/10.1177/0734904112459264

22. Hidalgo JP, Maluk C, Cowland A et al (2017) A Thin Skin Calorimeter (TSC) for quantifying irradiation during large-scale fire testing. Int J Therm Sci 112:383–394. https://doi.org/10.1016/j.ijthermalsci.2016.10.013

23. Tofilo P, Delichatsios MA, Silcock GWH, Shields TJ (2004) Wall heat fluxes in enclosure fires. In: Proceedings of 6th Asia-Oceania symposium on fire safety and technology, pp 108–119

24. Wickström U (2016) Temperature calculation in fire safety engineering. https://doi.org/10.1007/978-3-319-30172-3
25. Livkiss K, Andres B, Johansson N, van Hees P (2017) Uncertainties in modelling heat transfer in fire resistance tests: a case study of stone wool sandwich panels. Fire Mater . https://doi.org/10.1002/fam.2419
26. Johansson N, Svensson S, van Hees P (2015) A study of reproducibility of a full-scale multi-room compartment fire experiment. Fire Technol 51:645–665. https://doi.org/10.1007/s10694-014-0408-3
27. Peacock RD, Reneke PA, Davis WD, Jones WW (1999) Quantifying fire model evaluation using functional analysis. Fire Saf J 33:167–184. https://doi.org/10.1016/S0379-7112(99)00029-6
28. International Organization for Standardization (2015) ISO 5660-1, Reaction-to-fire tests—heat release, smoke production and mass loss rate—part 1: heat release rate (cone calorimeter method)
29. Babrauskas V (2016) The cone calorimeter. In: Hurley MJ, Gottuk DT, Hall JR Jr, Harada K, Kuligowski ED, Puchovsky M, Torero JL, Watts JM Jr, Wieczorek CJ (eds) SFPE handbook of fire protection engineering, 5th edn. Springer, p 952–980
30. McCaffrey BJ, Heskestad G (1976) A robust bidirectional low-velocity probe for flame and fire application. Combust Flame 26:125–127. https://doi.org/10.1016/0010-2180(76)90062-6
31. Sette BJ, Theuns E, Merci B, Vandevelde P (2007) Temperature effects on the mass flow rate in the SBI and similar heat-release rate test equipment. Fire Mater 31:53–66. https://doi.org/10.1002/fam
32. Hasemi Y, Yoshida M, Takashima S, Yokobayashi S (1996) Wall flame correlations and upward flame spread in a vertical channel and its relevance to fire safety. National Institute of Standards and Technology, Gaitherburg